Generation of attosecond pulse trains during the reflection of a very intense laser on a solid surface

Luis Plaja and Luis Roso

Departamento de Fisica Aplicada, Universidad de Salamanca, E-37008 Salamanca, Spain

Kazimierz Rzążewski

Center for Theoretical Physics and College of Science, Polish Academy of Sciences, Aleja Lotników 32/46, 02-668 Warsaw, Poland

Maciej Lewenstein

Commissariat à l'Energie Atomique, Centre d'Etudes de Saclay, 91191 Gif-sur-Yvette, France

Received December 17, 1997; revised manuscript received March 24, 1998

The normal-incidence reflectivity of a plasma generated on a solid surface by a very intense laser field is studied. We demonstrate that the reflected field has the form of trains of subfemtosecond pulses under suitable conditions. Particle-in-cell computations are presented and compared with a naïve moving-mirror model. The physical origin of this behavior is discussed in terms of the relativistic motion of the electron plasma.
 [S0740-3224(98)03807-7]
OCIS codes: 240.4350, 190.4160, 190.7110.

1. INTRODUCTION

The present exploration of the nonlinear nature of the coherent laser–matter interactions relies on the development of new sources of strong electromagnetic fields. In the quest for increasing the intensity, two complementary approaches have been developed. One of them, developed in relation with some nuclear fusion schemes, consists of gigantic lasers. The other consists of the time redistribution of the pulse energy. This technique, the so-called chirped-pulse amplification, consists of the expansion, amplification, and decompression of an initial pulse.[1] The present day refinement of chirped-pulse amplification techniques allows the generation of pulses with peak intensities close to 10^{20} W/cm^2, lasting for several femtoseconds. However, the achievement of shorter peaks will necessarily imply manipulating higher-harmonic frequencies and use of completely different schemes. In the present paper we want to discuss the feasibility of a different technique to obtain short pulses or, more precisely, not single short pulses, but trains.

Several proposals on how to reach the subfemtosecond limit have been put forward over the last few years. They all involve high-harmonic generation, mostly from gaseous media. There are essentially two types of proposals: (a) those that rely on phase locking between consecutive harmonics[2–5] and (b) those that concern single harmonics.[6,7] The first type of proposals exploits the fact that the harmonic spectra from a jet of rare gas exhibit a characteristic decrease for the first harmonics, followed by a plateau ended by a sharp cutoff.[8] In the plateau the spectrum consists of series of peaks of nearly equal amplitude. Farkas and Toth[2] indicated that, by filtering out N harmonics from the plateau, one could obtain a train of intense ultrashort pulses of duration $T/2N$, where T is the optical period, provided the harmonics were locked in phase. Although it does not turn out to be true on the level of individual atoms, phase locking can be induced by macroscopic propagation effects.[4] Moreover, by use of laser fields with time-modulated ellipticity, it should become possible to separate single ultrashort pulses from the train.[5] The proposal of Schafer and Kulander[6] employs very short fundamental phases (approximately 25–50 fs) that already lead to generation of very short harmonic pulses. Further compression can be achieved by compensating dynamically induced chirp of the harmonics.[9] Finally, Wahlström *et al.* combine the use of time-dependent ellipticity with the use of chirped fundamental pulses.[7] All of the above schemes are either experimentally complex or yield pulses of a limited power owing to the relatively low conservation efficiency of harmonic generation in gases.

It is the purpose of this paper to present the scheme of generation of attosecond pulse trains that are experimentally accessible. Our scheme is based on a different type of high-harmonic generation produced by laser pulses interacting with solid targets.[10–13] We show that the reflected signal, obtained in the case of normal incidence, has the form of a train of ultrashort pulses of duration 20 times shorter than the optical period (i.e., 100 attoseconds for the case of a Ti:sapphire laser). This could be surprising since on one hand the near-field harmonic spectrum is monotonically decreasing and does not exhibit any pla-

teau, while on the other hand, the production of those pulses does not require any filtering. The description of interaction of intense laser pulses with a solid target is in principle very complex and requires the use of particle-in-cell (PIC) codes.[14,15] Slowly emerging, however, is a relatively simple picture of this process. During the interaction of an intense short laser pulse with the solid surface a large number of electrons is released. The resulting layer of plasma does not have enough time to expand. Hence a dramatic electron-density gradient develops in which the density drops from a value corresponding to a solid to that of a vacuum in a distance much shorter than the wavelength of light. Thus an oscillating-mirror model has been proposed.[16–19] In the present paper, numerical PIC simulations will be presented and analyzed, and the underlying physical effects will be extracted with the help of a moving-mirror model. Our central result is that both PIC simulations and moving-mirror predictions qualitatively agree in getting a reflection mode made up of a train of short pulses. PIC simulations can be considered today as the state of the art in these kinds of problems, and the moving-mirror model allows a nice and direct interpretation of the physical underlying effects responsible for these trains of short pulses, although the moving-mirror concept, in the relativistic domain, needs some cautions.

2. PARTICLE-IN-CELL PLASMA CODES

When a multiterawatt laser field impinges on a solid target, an electron plasma is instantaneously created, and therefore the evolution of the field is influenced by the plasma. The state of the art simulations of a plasma interacting with a coherent field, in this context, are the so-called PIC simulations. In these simulations, electrons are described as classical particles that are accelerated to relativistic velocities by the Lorentz force. Quantum mechanical simulations in this regime are unfeasible. Therefore electron ionization is considered phenomenologically, assuming that free electrons appear almost instantaneously by overbarrier ionization.

We performed a realistic calculation based on a 1D3V PIC plasma code.[20,21] Our PIC code solves simultaneously the Maxwell equations and the relativistic Lorentz equation along a one-dimensional (1D) spatial coordinate, but including three dimensions in the velocity space. We assume a constant ion background, whereas the negative charges are described by moving finite-size particles. The integrations of the Maxwell equations is carried on in the reciprocal space using the charge and current densities derived from the charge distribution. Once the electromagnetic field is calculated for a given time, we integrate the Lorentz equation for the next time step. The 1D plasma simulated is typically a thin slab of width $\lambda/10$, which is discretized in cells of a few atomic units length, and $\sim 10^5$ negative particles are considered. The influence of a thicker slab will be briefly analyzed.

We assume that the driving laser field (incident from the left, as indicated in Fig. 1) is a monochromatic plane wave that oscillates like

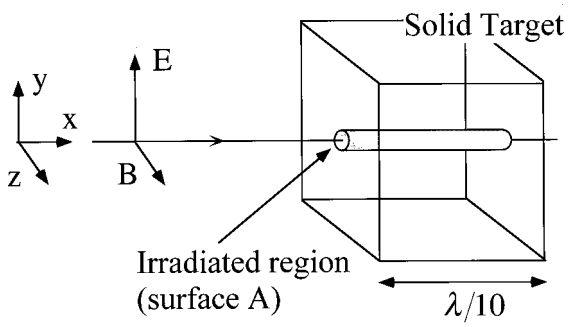

Fig. 1. Schematic representation of the geometry of the laser–plasma interaction studied. The laser beam is a linearly polarized plane wave that shines a thin foil. Only the normal incidence case is studied.

$$E_y(x, t) = E_0 f(t - x/c)\cos[\omega_L(t - x/c)],$$
$$B_z(x, t) = B_0 f(t - x/c)\cos[\omega_L(t - x/c)], \qquad (1)$$

where E_0 is the electric-field peak amplitude, B_0 is the magnetic-field peak amplitude, and ω_L is its frequency. We denote the direction of incidence by x, which we will often refer to as the longitudinal axis. The electric field is polarized along the y axis, and therefore the magnetic field is polarized along the z axis. Because we consider a plane wave in free space, electric- and magnetic-field amplitudes are related by $E_0 = B_0$. The pulse profile is described by a smooth function f. In the PIC simulations we have considered a $\sin^2$ turn on of five laser cycles and then a constant amplitude.

3. FAR-FIELD APPROXIMATION

Strictly speaking, a 1D plasma calculation describes the evolution of a system independent of the transversal coordinates. Therefore every particle must be thought as representing an infinite charged slab in the transversal direction. As a consequence, the Coulomb field between two 1D particles does not show the x^{-2} dependence as in the case of pointlike three-dimensional (3D) particles, but does show the law of constant field between the capacitor plates. This should be a good approximation for the internal plasma field, as long as the laser-focus spot size can be considered infinite in comparison with the thickness of the plasma, as in the cases considered here. The situation, however, is completely different if we would like to compute the field reflected at a distant point of the plasma surface. As long as this distance, R, is greater than or of the order of the focus characteristic length, the 1D approximation becomes inadequate for calculating the far field. For this case we can approximate the interaction region by a cylinder whose base area is the focus area, A. It is reasonable to assume that the plasma dynamics inside the interaction region is well described by the 1D model, while the plasma outside this region is unperturbed. With this in mind we compute the far field reflected by adding the individual contribution of each 1D charge, according to the standard expression[22]

$$\mathbf{E}_n(x, t) \approx \frac{A}{cR} q_n \left[\frac{\mathbf{e}_x \times \{\mathbf{e}_x + \boldsymbol{\beta}_n\} \times \dot{\boldsymbol{\beta}}_n}{(1 + \boldsymbol{\beta}_n \cdot \mathbf{e}_x)} \right]_{\text{ret}}, \qquad (2)$$

where the subindex n labels the 1D charge, which has units of a surface density in the 3D space, and provided the term enclosed by square brackets is computed at the retarded time $t - R/c$. Since the observation-point distance is much larger than the plasma width, we have taken a constant R for all the charges. With the approximations made, the angular distribution of the scattered field follows the diffraction pattern of a puntual source; i.e., it is extended over the whole solid angle.

Despite the fact that the electron cloud is expanding, the transverse area of the cloud, A, is assumed to be constant, because the interaction times we are interested in are extremely short (subpicosecond).

It is worth pointing out that near and far fields have different spectra. Near- and far-field harmonic spectra differ in the relative amplitudes of the harmonics. This is important for our result. Trains of short pulses need two conditions to appear: first, a locking of the relative phases, which is achieved both in the near and in the far fields; second, a given sequence of amplitudes, which is not fulfilled by the near field. This will be analyzed in detail at the end of the paper.

4. PARTICLE-IN-CELL SIMULATIONS

We compute the plasma response and the generated fields for several cases. Before we turn to the presentation and discussion of the simulations, let us consider the parameter regime of interest.

We chose the typical wavelength of the Ti:sapphire laser, 800 nm, i.e., to laser frequency 0.057 a.u., or to photon energies close to 1.55 eV. We shall consider laser intensities up to 10^{20} W/cm^2, i.e., several thousands of atomic units of intensity. This is a very high but already feasible value of the intensity.[23] The most interesting regime of values of the electron density (measured in terms of the plasma frequency ω_p) should correspond to the vicinity of the critical regime $\omega_p = \omega_L$. The simple explanation of this fact is that, as an ultraintense laser pulse interacts with the solid surface, it causes ionization and rapid increase of the electron density. However, as soon as some regions of the solid target reach density values higher than the critical value, the laser light will not be able to propagate through and penetrate those regions. Therefore plasma densities with $\omega_p > \omega_L$, over critical densities, are reasonable only if considering a metal with a high density of free electrons, and are not expected to be generated by strong field ionization. The case $\omega_p > \omega_L$ presents the advantage of a greater binding of the electrons and a faster restoring frequency. We will compare numerical PIC results involving critical and overcritical regimes.

Figure 2 shows numerical PIC simulation for the laser parameters $E_0 = 25$ a.u. (intensity of 2×10^{19} W/cm^2) and $\omega_L = 0.057$ a.u., but for a plasma density 16 times greater than the critical density, i.e., $\omega_p = 4\omega_L$. This corresponds to a density of 3×10^{22} electrons/cm^3. Figure 2(a) shows the reflected-field time-dependent profile, $E_R^2(t)$, calculated from Eq. (2), in the far-field region at a distance R of the thin film. Intensity is rescaled by $(R/A)^2$ to account for such distance and for the thin-film area, A. The plotted values can be associated with the intensity profile, provided we multiply by the $(A/R)^2$term, corresponding to the particular experimental conditions. Amazingly, the profile is a subfemtosecond pulse train. Figure 2(b) shows the time evolution of the electronic plasma-cloud density $\rho^2(x, t)$, along the x axis, for these parameters. Electron density is indicated by a gray scale rescaled to the equilibrium density. Dark regions correspond to high electronic density. The oscillation of the electrons is clearly apparent. Initially they are uniformly distributed over a slab λ/10, 80 nm, thick. During the few first cycles, plasma oscillates in very regular forms, allowing the formation of the short peaks. After ten cycles, many electrons show large amplitude trajectories that expend well into the vacuum. Since the plasma density if 16 times bigger than the critical density, electrons are tightly bounded to the positive ions with a restoring force strong enough to delay the explosion of the plasma.

One clear way to avoid the effect of plasma expansion is to reduce the time scale and the excursion length by the use of higher frequencies. We computed results for the laser frequency, $\omega_L = 0.228$ a.u., that correspond to a wavelength of ~200 nm. This is the fourth harmonic of

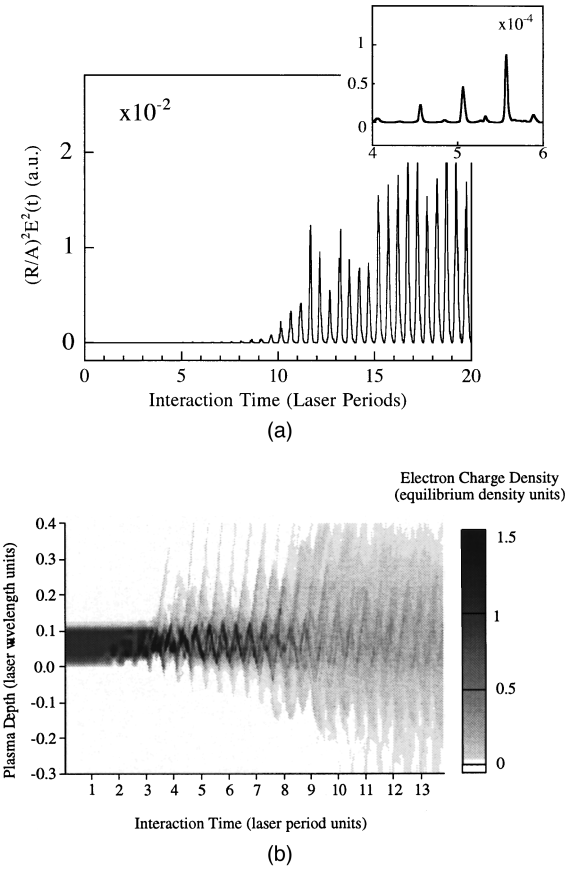

Fig. 2. Numerical PIC simulation for a feasible set of laser parameters, $\omega_L = 0.057$ a.u., $E_0 = 25$ a.u., and for an overcritical plasma density, $\omega_P = 4\omega_L$. (a) Time-dependent intensity profile, or more precisely, the time dependence of the electric-field amplitude square, $E_y^2(t)$, in the far-field region, at a distance R of the thin film. Intensity is rescaled by $(R/A)^2$ to account for the distance and for the thin-film area. (b) Time evolution of the electronic plasma-cloud density $\rho^2(x, t)$, along the x axis, for these parameters.

the previously considered case and perhaps is not the best possibility from the experimental point of view. Note, however, that this frequency is a good choice for the numerical simulations and the discussion of the dynamics in two very different regimes. In this case we can move to critical-density plasmas, $\omega_P = \omega_L = 0.228$ a.u. This corresponds to an electron density 3×10^{22} electrons/cm^3, the same density as in the previous case. The solid slab thickness has to be proportionally reduced. To check this, we made a PIC computation for a slab λ, $\lambda \approx 200$ nm thick. Results are shown in Fig. 3, that correspond to laser parameters $E_0 = 55$ a.u. (intensity of 10^{20} W/cm^2) and $\omega_L = 0.228$ a.u. The thickness of the slab prevents the regular oscillation of the electrons; some waves appear but not regularly enough to generate short pulses. Therefore thickness has to be reduced. Figure 4 corresponds to $\lambda/10$, 20 nm, for the same laser parameters and electronic density as in Fig. 3. Now the profile is again a train of pulses, and the electron cloud oscillates in a very regular way over more than 10 laser cycles, although eventually the electron cloud will expand enough to degrade the quality of the surface of the film. The time domain of clear oscillatory motion matches the zone of clearly defined peaks. When the peaks disappear (the incident field is being constant), the plasma has expanded from the vicinity of the film. The surface degradation owing to the extension of the plasma-charge trajectories into the vacuum begins to appear at the high intensities considered in this paper. For weak radiation the amplitude of the particles' oscillations is much smaller, and therefore plasma surface degradation is not severe. This can be seen in calculations with electric fields of the order of a few atomic units.[17] Therefore it is expected that the presence of a pedestal in the ultrahigh intensity laser, which lies orders of magnitude below the peak intensity, will not induce surface degradation before the central pulse arrives.

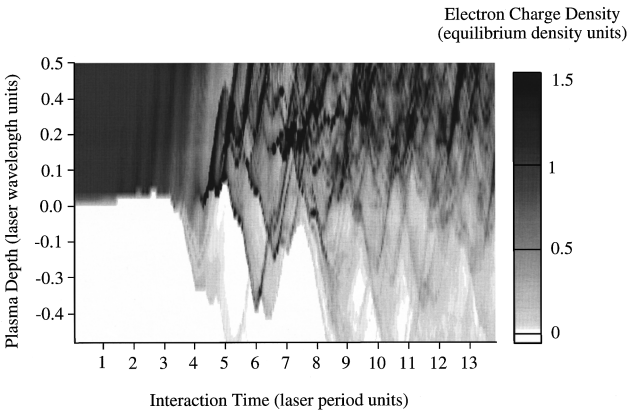

Fig. 3. Numerical PIC simulation for laser frequency $\omega_L = 0.228$ a.u. and amplitude $E_0 = 55$ a.u. (intensity 10^{20} W/cm^2) and for a critical density, $\omega_P = \omega_L$. The slab is now one wavelength 200 nm thick. Only the time evolution of the electronic plasma-cloud density $\rho^2(x, t)$, along the x axis, is shown. Clearly the oscillation of the electrons is not regular. The time-dependent intensity profile does not show narrow peaks for these parameters.

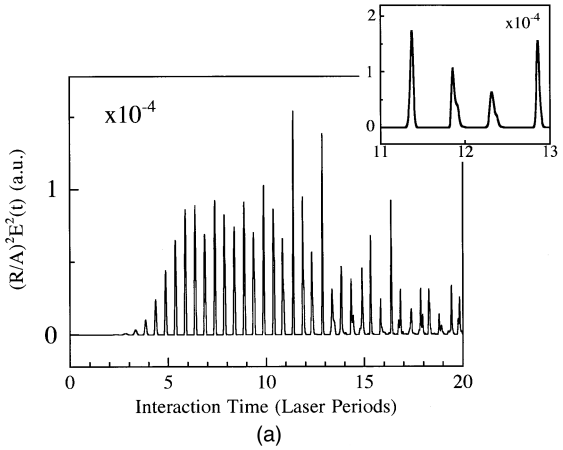

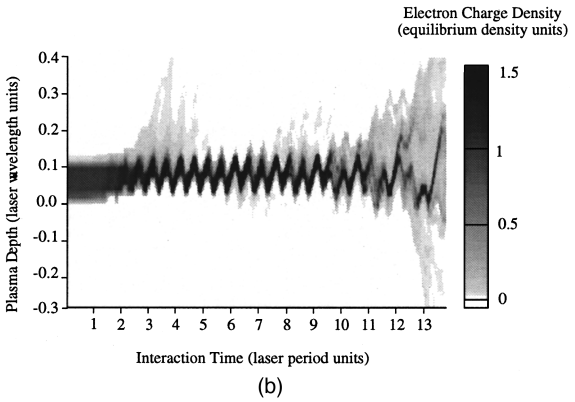

Fig. 4. Numerical PIC simulation for laser frequency $\omega_L = 0.228$ a.u., amplitude $E_0 = 55$ a.u. (intensity 10^{20} W/cm^2), and critical density $\omega_P = \omega_L$, the same parameters as in the previous figure. Now the thickness of the slab has been reduced to $\lambda/10$, 20 nm. This reduction is enough for the reappearance of the train of short peaks. (a) Time-dependent intensity profile. (b) Time evolution of the electronic plasma-cloud density $\rho^2(x, t)$, along the x axis. Now the regular sequence of peaks last longer than in Fig. 2 because of the short frequency of the laser, but eventually all electrons leave the solid vicinity.

5. NAÏVE MOVING-MIRROR MODEL

In the simplest case the linearly polarized pulse impinges upon the oscillating thin layers of electrons at normal incidence. It is reasonable to assume that there is no significant absorption in the target and that the reflection of the pulse is perfect. Such assumption is equivalent to treating the oscillating surface as the surface of a perfect conductor and to adopting the corresponding boundary conditions in Maxwell equations.

The motion of the surface corresponds to the motion of the electrons in the layer in the direction perpendicular to the surface. Thus this motion combines the effects of the Lorentz force, the relativistic mass correction, and the restoring force in the x direction owing to plasma oscillations. Equations of motion for the mirror then read

$$\frac{d\mathbf{p}}{dt} = q\mathbf{E}(\mathbf{r}, t) + \frac{q}{c}\mathbf{v}\wedge\mathbf{B}(\mathbf{r}, t) - m\omega_P^2 x, \qquad (3)$$

$\mathbf{p}$ being the relativistic momentum. It is useful to define the relativistic velocity, $\mathbf{u} = \gamma\mathbf{v}$, where $\gamma = (1 + u^2/c^2)^{1/2}$ is the standard parameter to account for the relativ-

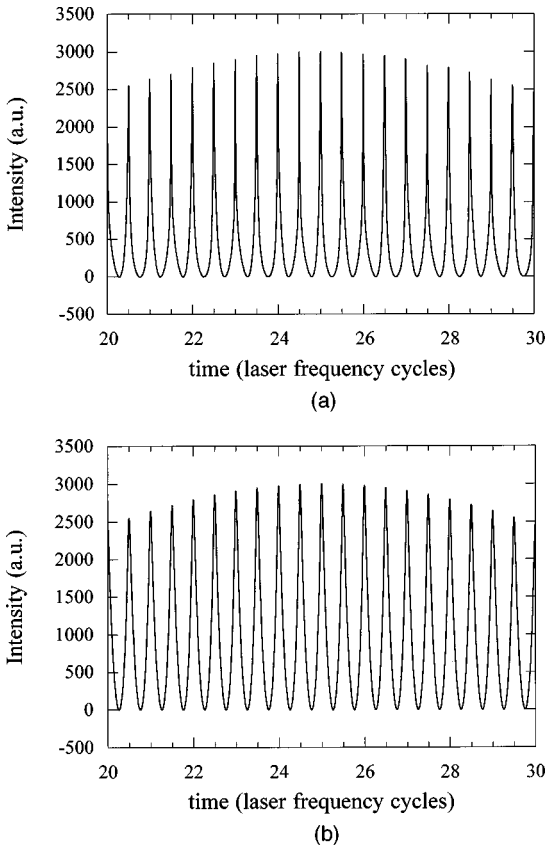

Fig. 5. Time profile for the reflected intensity $E_R^2(t)$ depicted for an incident pulse with a $\sin^2$ envelope and with a total duration of 50 cycles. The incident amplitude peak is $E_0 = 55$ a.u. (intensity of 1×10^{20} W/cm^2). The electron density for these drawings is exactly equal to the critical density, $\omega_P = \omega_L$. (a) $\omega_L = 0.057$ a.u., a result that is not realistic. (b) $\omega_L = 0.228$ a.u., which agrees with PIC simulation.

istic effects. With this notation, and introducing only the nonvanishing components of electric and magnetic fields, one gets

$$\frac{du_x}{dt} = +\frac{q}{\gamma mc} u_y B_z(x, t) - \omega_P^2 x,$$

$$\frac{du_y}{dt} = \frac{q}{m} E_y(x, t) - \frac{q}{\gamma mc} u_x B_z(x, t). \quad (4)$$

Once the velocity is calculated, the position of the particle, $s_x(t)$ and $s_y(t)$, is trivially given by integration of $v_x = ds_x/dt$ and $v_y = ds_y/dt$. In the moving-mirror model we consider that all electrons move with exactly the same velocity and that all started from $s_x = 0$. Therefore they constitute a plane that is oscillating according to the Lorentz and plasma forces. It is the moving mirror. The reflected field E_R may be obtained from the requirement of vanishing of the total electric field at the electron surface $s_x(t)$,

$$E_R[t - s_x(t)/c] + E_0 \cos\{\omega_L[t + s_x(t)/c]\} = 0. \quad (5)$$

The plasma frequency depends explicitly on the electronic density, and thus implicitly on the electronic dynamics, degree of ionization, etc. Although it does therefore depend on the laser field itself, we will consider it in the following as an independent parameter.

Results of the moving-mirror model are shown in Fig. 5. In this figure the temporal reflected intensity profile $I(t) = E_R^2(t)$ is depicted for an incident pulse with a $\sin^2$ envelope and a total duration of 50 cycles. The incident amplitude peak is $E_0 = 55$ a.u. (intensity of 1×10^{20} W/cm^2). The electron density for these drawings is exactly the critical density, $\omega_P = \omega_L$. Figure 5(a) corresponds to the frequency $\omega_L = 0.057$ a.u. In this case the amplitude oscillation is too big, and the moving-mirror result does not give a realistic result. Figure 5(b) corresponds to $\omega_L = 0.228$ a.u. In this second case the amplitude of the oscillation of the electrons is not as big as in the previous case, and therefore the simplified model for the restoring can be more realistic. Results are in agreement with the simulations of Fig. 4.

6. ELECTRON TRAJECTORIES

To extract conclusions on the physical origin of this particular generation of short peaks, we propose to analyze the dynamics of the electrons in the plasma.

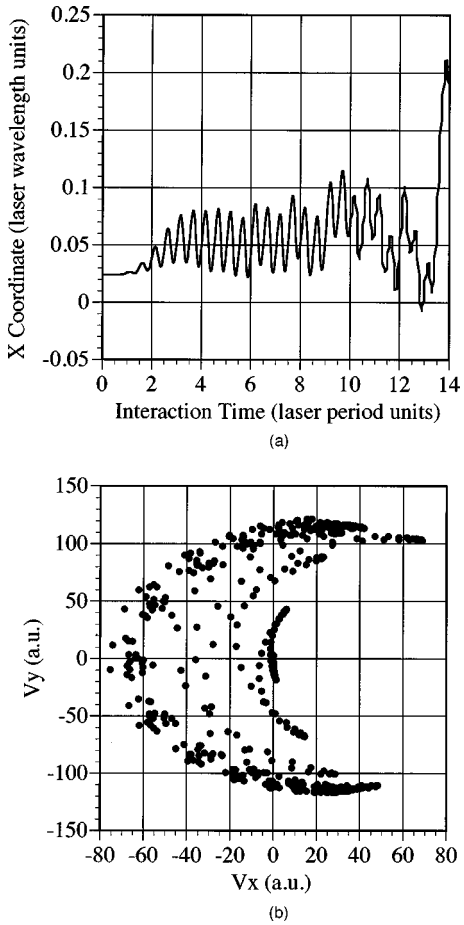

Fig. 6. Motion of one selected electron in the plasma for the same parameters as Fig. 4, $\omega_P = \omega_L = 0.228$ a.u. and $E_0 = 55$ a.u., extracted from the PIC simulation. Only one electron trajectory is selected that shows what can be called a typical trajectory. (a) Longitudinal coordinate as a function of time. (b) Longitudinal velocity, v_x, as a function of its transversal velocity, v_y.

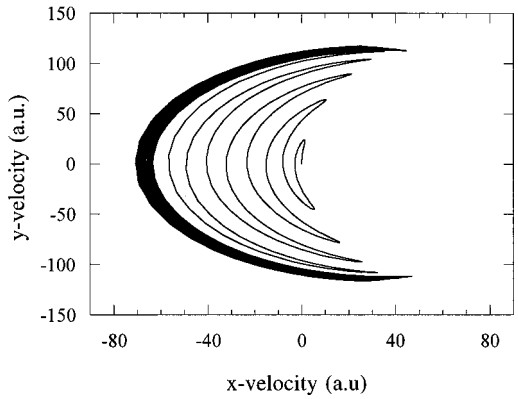

Fig. 7. Electron dynamics calculated from the Lorentz force as indicated in Eq. (3). The figure shows the longitudinal velocity, v_x, as a function of the transversal velocity, v_y, for the same parameters as in Fig. 6. The similarity with Fig. 6(b) is remarkable, and this is the reason of the validity of the moving-mirror result for these parameters. Observe the proximity of the speed of light limit, $c = 137$ a.u., indicating the necessity of a relativistic description of the dynamics.

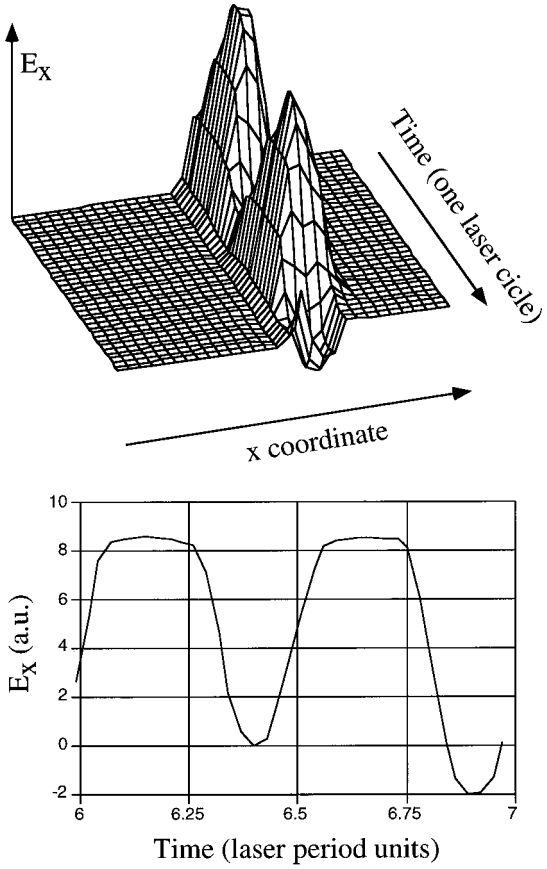

Fig. 8. Longitudinal electric field $E_x(x, t)$ at each point of the longitudinal coordinate calculated with the PIC code for an incident amplitude $E_0 = 55$ a.u., frequency $\omega_L = 0.228$ a.u., and critical density $\omega_P = \omega_L$. (a) Spatio-temporal profile for one cycle. (b) Cut at a convenient value of the x coordinate.

Figure 6 shows the motion of one electron in the plasma for the case of Fig. 4: $\omega_P = \omega_L = 0.228$ a.u. and $E_0 = 55$ a.u. Of course, only one electron has been selected that shows what can be called a typical trajectory, i.e., one of those electrons oscillating for several cycles and eventually leaving the film. Figure 6(a) shows this oscillation, which lasts more or less regularly for 12 cycles. Figure 6(b) shows the velocities, owing to the driving of the electric field; the transverse component is very close to the speed of light, $c = 137$ a.u., and the longitudinal velocity is asymmetric in the positive and negative directions. This is just the origin of the generation of short peaks by the oscillating mirror.

To compare with the mirror model, we computed the trajectory given by the Lorentz force equation (3). The result, for the same parameters, is shown in Fig. 7, which agrees quite well with Fig. 6(b).

However, the agreement is not as good for other regimes. It is not completely understood by us, but there is some evidence that PIC simulations give trains of short peaks in many situations where the moving-mirror model does not predict such behavior. One of these cases is described in Fig. 8, where the longitudinal electric field $E_x(x, t)$ at each point of the longitudinal coordinate is represented, for an incident amplitude $E_0 = 55$ a.u., frequency $\omega_L = 0.228$ a.u., and critical density $\omega_P = \omega_L$. The spatio-temporal profile is shown in Fig. 8(a), for one cycle (selected after the turn-on in the region of nice oscillatory behavior). Of course, the longitudinal field vanishes out of the plasma. Inside the plasma, however, this longitudinal component can provide a clear physical insight of the electron dynamics. The electric field presents several nice features. First, the field average is not zero but a positive value, owing to the shift of the center of mass of the negative cloud. Second, the oscillations are not sinusoidal; they present, instead, a flat top owing to the nonharmonic character of the restoring force. This can be clearly seen in Fig. 8(b), which simply is a cross section of Fig. 8(a), at a convenient value of the X coordinate. In our opinion this proves that the moving-mirror model is a nice model to start with, but the results obtained may be unrealistic in many situations. The restoring force in a real case is not harmonic and, moreover, electron collisions cannot be neglected.

7. RELATION TO HIGH-ORDER HARMONICS

The narrowing of the pulse duration becomes dramatic when E_0 is sufficiently large, i.e., when the motion of electrons becomes highly relativistic. Even though harmonic generation from solid surfaces has been discussed in the literature,[10–13] its potential for generating ultrashort pulses has been overlooked. Ultrashort-pulse generation is usually associated with phase-locking phenomenon,[24] when several harmonic modes of similar amplitude add in phase. This is in fact the mechanism of attosecond pulse-train generation in gases, where the macroscopic propagation induces the phase locking of several harmonics from the plateau of the spectrum.[4] In the case of generation from a solid target in the regime of parameters considered here, there is no well-developed plateau in the harmonic spectrum. Nevertheless, the harmonics are from the very beginning locked in phase, and their strength decreases sufficiently slowly with their order, so that the resulting temporal signal consists of a train of ul-

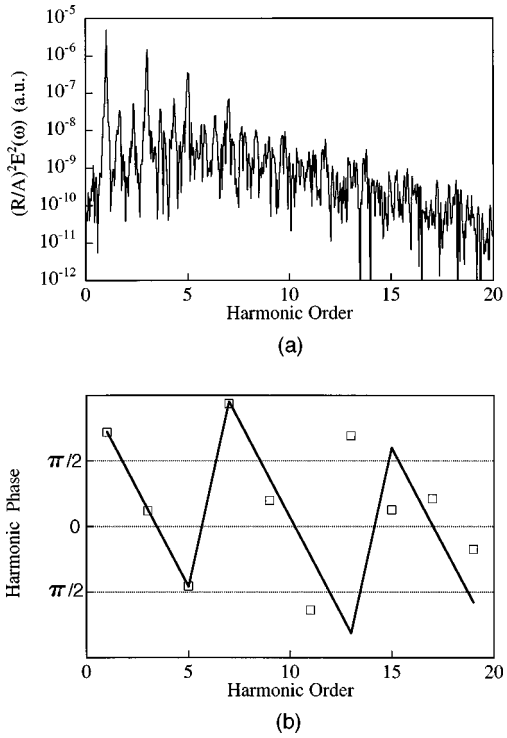

Fig. 9. Harmonic spectrum of the reflected far field computed in the PIC simulation for laser frequency $\omega_L = 0.228$ a.u., amplitude $E_0 = 55$ a.u. (intensity 10^{20} W/cm^2), critical density $\omega_P = \omega_L$, and slab thickness equal to $\lambda/10$, 20 nm, which are the same parameters as in Fig. 4, where a nice train of short pulses appeared. (a) Intensity spectrum, (b) phases of the harmonics.

trashort pulses. This is shown in Fig. 9, which corresponds to the same parameters as the case shown in Fig. 4: laser frequency $\omega_L = 0.228$ a.u., amplitude $E_0 = 55$ a.u. (intensity 10^{20} W/cm^2), critical density $\omega_P = \omega_L$, and slab thickness equal to $\lambda/10$, 20 nm, where a nice train of short pulses appeared. Figure 9(a) shows the intensity spectrum and Fig. 9(b) shows the phases of the harmonics. Small squares in Fig. 9(b) indicate the phases of the different harmonics, and the solid curve is drawn to show the clear linear dependence of the phases of the first ten harmonics. The harmonics that do not follow this line lie down the background noise and thus are not significant. Therefore phase locking is clear up to the tenth harmonic, and attosecond trains are expected of width roughly equal to one tenth of the laser period.

There exists, however, a much clearer physical explanation of this effect in the framework of the oscillating-mirror model. As the velocity of the mirror becomes comparable to the light velocity, one approaches the shock-wave instability (in which, as in a sonic boom, for example, the velocity of the source becomes comparable to the phase velocity of the wave). The above results suggest that harmonic generation from solid surfaces might be the best source of attosecond pulses and the best playground for the attosecond physics.

The presence of a noisy background radiation in the spectra is a signature that the dynamics of the system is more complicated than that of the moving mirror. For instance, when the plasma is highly overcritical, surface charges follow irregular trajectories, possibly chaotic. Therefore it is our belief that the background radiation induced by these irregularities has an incoherent nature.

Since the spectrum is calculated from the scattered field written in Eq. (2), the harmonic intensity for a given experimental condition must be calculated from the values plotted in Fig. 9(a), multiplied by $(A/R)^2$, A being the area of the laser focal spot and R being the distance between the detector and the plasma surface. The relatively low intensity of the harmonic yield for the numerical simulations in comparison with the value predicted by the moving mirror stands for the fact that Eq. (2) corresponds to the diffraction pattern of a point source. Therefore the harmonic intensity is spread over the whole solid angle. Also, in the case of the moving mirror, we assume a perfectly reflecting plasma, which is certainly not realistic for the thin plasma considered in the numerical simulations.

8. CONCLUSIONS

In conclusion we have developed a PIC code 1D in space and 3D in velocity, and where the ions are kept fixed. We used this code to describe the dynamics of a thin electron plasma driven by a laser field at normal incidence and for intensities where the dynamics is relativistic. The reflected field, in the far-field regime, is computed for several situations. The surprising new result is the appearance of trains of subfemtosecond peaks in the reflected field. Because of the apparent generality of our description, this can be regarded as a completely new procedure to generate short peaks. The physical origin of those peaks is related to the composition of several harmonics with phase locking, but can be more easily understood in terms of a moving mirror. Many details of the physical origin of these trains of peaks are not completely clear. The moving-mirror model fails in many cases, because of the expansion of the electronic cloud, and shows dephasings because of the rigid character of the restoring force. Within the PIC simulation, results show an expanding electron plasma that eventually escapes from the positive charges, but that has enough time to generate such trains. Neglecting ion expansion is a reasonable approximation for few-cycles-long pulses. Laser parameters used in these computations are realistic for the most intense lasers at present, particularly for the 800-nm case.

ACKNOWLEDGMENTS

We acknowledge enlightening discussions with Th. Auguste, P. Monot, and A. Pukhov. K. Rzążewski acknowledges support of KBN grant 2P03 B04209. Partial support from the Spanish Dirección General de Investigación Científica y Técnica (grant PB95-0955), the Junta de Castilla y Leon (grant SA37/97), and the European Commission Training and Mobility of Researchers Program (under contract ERBFMRXCT96-0080) is acknowledged.

REFERENCES AND NOTES

1. See feature issue on high-field interactions and short wavelength generation, J. Opt. Soc. Am. B **13**, 51 (1996).

2. G. Farkas and C. Toth, Phys. Lett. A **168**, 447 (1992).
3. S. E. Harris, J. J. Macklin, and T. W. Hansch, Opt. Commun. **100**, 487 (1993).
4. Ph. Antoine, A. L'Huillier, and M. Lewenstein, Phys. Rev. Lett. **77**, 1234 (1996).
5. P. B. Corkum, N. H. Burnett, and M. Y. Ivanov, Opt. Lett. **19**, 1870 (1994); M. Yu. Ivanov, P. B. Corkum, T. Zuo, and A. Bandrauk, Phys. Rev. Lett. **74**, 2933 (1995).
6. K. J. Schafer and K. C. Kulander, Phys. Rev. Lett. **78**, 638 (1997).
7. C.-G. Wahlström, in *Multiphoton Processes VII*, P. Lambropoulos and H. Walther, eds. (Institute of Physics, London, 1997), pp. 160–167.
8. J. J. Macklin, J. D. Kmetec, and C. L. Gordon, III, Phys. Rev. Lett. **70**, 766 (1993); A. L'Huillier and Ph. Balcou, Phys. Rev. Lett. **70**, 774 (1993).
9. This idea has been also discussed by P. Salières, Ph.D. dissertation (Université Paris VI, Paris, 1995).
10. For early work with CO_2 lasers, see R. L. Carman, D. W. Forslund, and J. M. Kindel, Phys. Rev. Lett. **46**, 29 (1981).
11. S. Kohlweyer, G. D. Tsakiris, C. G. Wahlström, C. Tillman, and I. Mercer, Opt. Commun. **117**, 431 (1995).
12. D. von der Linde, T. Engers, G. Jenke, P. Agostini, G. Grillon, E. Nibbering, A. Mysyrowicz, and A. Antonetti, Phys. Rev. A **52**, R25 (1995).
13. P. A. Norreys, M. Zepf, S. Moustaizis, A. P. Fews, J. Zhang, P. Lee, M. Bekarezos, C. N. Danzos, A. Dyson, P. Gibbon, P. Loukakos, D. Neely, F. N. Wajsh, J. S. Wark, and A. E. Angor, Phys. Rev. Lett. **76**, 1832 (1996).
14. P. Gibbon, Phys. Rev. Lett. **76**, 50 (1996).
15. A. Pukhov and J. Meyer-ter-Vehn, Phys. Rev. Lett. **76**, 3975 (1996).
16. S. V. Bulanov, N. M. Naumova, and F. Pegoraro, Phys. Plasmas **1**, 745 (1994).
17. R. Lichters, J. Meyer-ter-Vehn, and A. Pukhov, Phys. Plasmas **3**, 3425 (1996).
18. D. von der Linde and K. Rzążewski, Appl. Phys. B: Photophys. Laser Chem. **63**, 499 (1996).
19. S. Kohlweyer and G. D. Tsakiris, *ICOMP VII*, P. Lambropoulos and H. Walther, eds. (Max Planck Institute fur Quantenoptik, Garching, 1996); Abstract B34.
20. J. M. Dawson, Rev. Mod. Phys. **55**, 403 (1983).
21. C. K. Birdsall and A. B. Langdon, *Plasma Physics Via Computer Simulation* (Institute of Physics, London, 1991).
22. J. D. Jackson, *Classical Electrodynamics* (Wiley, New York, 1975).
23. 6×10^{19} W/cm^2 has been obtained at Ensta (Paris). J. P. Chambaret, LOA, Ensta, Palaiseau, France (personal communication).
24. A. E. Siegmann, *Lasers* (University Science, Mill Valley, Calif., 1986).